A Nanoscale Composite Material for Enhanced Damage Tolerance in MEMS Applications

A. Paranjpye, Noel C. MacDonald, Glenn E. Beltz

Department of Mechanical and Environmental Engineering,
University of California, Santa Barbara 93106

ABSTRACT

A two-dimensional laminar composite material has been shown [1] to exhibit enhanced damage tolerance due to zones of residual compressive stress. The damage tolerance appears as a threshold stress below which the structure does not fail catastrophically. We utilize this concept at the microscale, towards obtaining fracture resistant MEMS structures. Cantilever beams of this laminar composite material, manufactured by MEMS fabrication methods are deflected to fracture, and the measured fracture strength compared to single crystal silicon beams (SCS) of identical geometry. All structures are made on the same die, so uniform processing damage is likely for all of them. A wide range of fracture strength is seen in both the composite and SCS beams. However, the lowest value of fracture stress for all the composite beams is found to be above the predicted threshold strength, while some of the SCS beams fail at lower stresses. We conclude that this composite offers a useful design alternative as a MEMS material.

Keywords: MEMS, silicon, damage tolerance, composite

1 BACKGROUND

Brittle materials, like glasses and ceramics often undergo catastrophic failure with little or no warning even when stressed at levels below their elastic limit. These materials typically have no mechanisms that allow the rearrangement of atoms into more stable configurations to accommodate the applied load. Therefore, any flaw in the material structure that builds up a stress concentration around it can serve as the precursor to a crack. Such cracks can extend catastrophically through the entire structure to cause failure even though the applied stress may be well below the level to rupture atomic bonds. The failure strengths of these materials can be characterized probabilistically at best, since it is not possible to know the size, shape, position and orientation of every single flaw in the structure. Designing structures using these materials becomes a challenge, and proof testing of each component to the design load becomes necessary when the cost of failure is high.

Single Crystal Silicon, the material of choice for many bulk micromachined Micro-Electro-Mechanical Systems (MEMS), suffers from the bane of brittle materials, i.e. a low fracture toughness of 0.9 $MPa.m^{1/2}$ [2] and a sharp transition from elastic deformation to fracture. This effect is exacerbated by the presence of residual stresses and surface flaws from processing MEMS devices, which can lead to brittle behavior and a non-deterministic strength for finished structures. An earlier attempt to develop MEMS microsurgery tools was aborted when the finished devices failed unpredictably during testing. The low fracture toughness of silicon makes a silicon flexure susceptible to failure under almost any kind of shock or impact loading. As another example, in a micro aerial vehicle development project, [3] silicon was rejected as a material for the wing frames in favor of metal because the wings shattered every time the MAV crash-landed.

Regions of residual compressive stress in a material can be effective at improving material reliability by acting as "crack traps" because the driving force for extending a crack is lowered when a crack enters one of these zones. Specifically, thin compressive layers within a laminar bimaterial ceramic have been shown [1] to be effective at trapping large surface and internal cracks. The damage tolerance and reliability of the materials is manifested in terms of a threshold stress below which the probability of failure is zero. Mathematical modeling and finite element analysis of this geometry [4] shows that reducing the size scale of these compressive zones and their separation enhances the damage tolerance phenomenon.

Microfabrication technology employed for MEMS fabrication allows structures to be made with minimum feature sizes in the sub-micron to 100-nm size range. Consequently, a high threshold stress can be achieved, and this approach could present a useful means for improving upon the mechanical properties of bulk micromachined devices. The process flow envisaged allows a MEMS device, or critical stressed zones in a device e.g. flexures to be fabricated from this material using standard microfabrication techniques, without requiring a new substrate material or etching techniques and tools.

2 DAMAGE TOLERANCE MODEL

Rao [1] developed a model for estimating the stress intensity factor at the tip of a crack running across multiple layers of a laminate composite structure with alternating layers of residual biaxial compressive and tensile stress. The residual stresses may evolve due to a differential

thermal expansion coefficient, a phase transformation, an increase in molar volume due to a chemical reaction or, in general, any phenomenon that leads to a strain mismatch between layers. Their analysis assumes a crack of length 2a extending across a tensile layer and into the two neighboring compressive layers. The stress intensity factor obtained is equated to the fracture toughness of the compressive layer material to obtain an expression for the threshold stress.

$$\sigma_{thr} = \frac{K_c}{\sqrt{\pi \frac{t_2}{2}(1+\frac{2t_1}{t_2})}} + \sigma_c \left[1-\left(1+\frac{t_1}{t_2}\right)\frac{2}{\pi}\sin^{-1}\left(\frac{t_2}{t_2+2t_1}\right)\right] \quad (1)$$

where:

$a \rightarrow$ length of crack

$\sigma_a \rightarrow$ applied tensile stress

$\sigma_c \rightarrow$ residual compressive stress

$t_1, t_2 \rightarrow$ compressive and tensile layer widths

$K_c \rightarrow$ critical stress intensity for compressive layer material

The material system under consideration consists of alternating thin layers of silicon dioxide with a residual biaxial compressive stress sandwiched between thicker layers of silicon with a residual biaxial tensile stress. The strain mismatch originates from the differential thermal expansion coefficient of the two materials, as the system is cooled from the process temperature to room temperature. The relevant material properties are shown in Table 1.

Material	CTE ($x10^{-6}$/°C)	Young's Modulus (GPa)	Poisson's Ratio	Fracture Toughness K_c (MPa.m$^{1/2}$)
Silicon	2.60	130	0.25	0.9
SiO_2	0.50	50	0.16	1.0

Table 1: Material Properties for Si-SiO_2 system

For a Si-SiO_2 composite, the strain mismatch is assumed to start to build up below 960°C, the glass transition temperature. The maximum residual compressive stress that can be generated is ~208 MPa, which is relatively low. From (1), we can see that the threshold stress depends primarily on two factors, the magnitude of the residual compressive stress, and inversely with the size scale of the layers. The compressive stress generated depends upon the elastic coefficients of the two materials, and the strain mismatch. Since none of the other factors are under experimental control, reducing the size scale of the layer widths and optimizing the layer width ratio, becomes the primary route to obtaining a high threshold stress. The minimum size scale that can be fabricated is dictated by technological considerations. By using electron beam lithography and high plasma power etching tools, layer widths as small as 50-100 nm can be fabricated. Figure 1 shows predicted variance of the threshold stress with layer size scale.

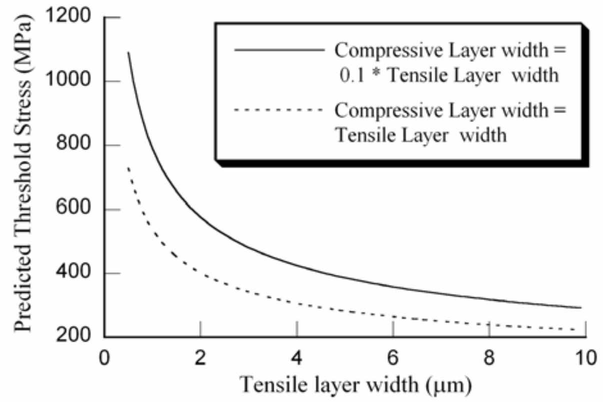

Figure 1: Predicted threshold stress for microcomposites

3 EXPERIMENT

Bulk silicon microfabrication techniques were used to fabricate cantilevers of this composite material. Monolithic silicon cantilevers are fabricated on the same die along with the composite cantilevers to compare the fracture strengths of the two materials. Each cantilever is 1.5mm long, 2mm wide and 40 μm deep and consists of a large number of alternating layers of silicon and thermally grown silicon oxide.

Tensile Layer		Compressive Layer		Predicted Threshold Strength (MPa)
Thickness (μm)	Residual Stress (T)(MPa)	Thickness (μm)	Residual Stress (C)(MPa)	
1.713	86.41	1.787	82.83	**394**
4.213	41.65	1.787	98.20	**333**
14.213	13.56	1.787	107.84	**225**
3.426	86.41	3.574	82.83	**293**
8.426	41.65	3.574	98.20	**250**
28.426	13.56	3.574	107.84	**170**

Table 2: Geometry and properties of fabricated cantilevers

The layer widths, as well as their ratio are varied to explore the effect of these parameters on the crack arrest properties. Each die consists of two sets of cantilevers, each set having a constant compressive layer thickness and with tensile layers of different thickness. A table of the various geometries fabricated, along with the fracture properties predicted from the model is shown in Table 2.

3.1 Microfabrication Process

After patterning the mask oxide, the silicon beams are etched by Deep Reactive Ion Etching (DRIE) using the Bosch process. The wafers are then thermally oxidized at 1100°C in steam. When silicon is oxidized, the resulting SiO_2 occupies a larger volume (2.27 times) than the silicon

it consumes. This effect is utilized to fill the gaps between the silicon beams to form a material block of the laminar composite. A high temperature (1100°C) anneal allows the SiO_2 grown from both sides of the trench to flow and form a SiO_2 layer without an interface running midway through it. When cooled to room temperature, the differential thermal expansion between the Si and SiO_2 layers causes the residual stresses. The residual stresses, however, only build up below ~960°C, the glass transition temperature of SiO_2, below which it ceases to flow. A pattern of vias is then aligned with the cantilevers on the backside of the wafer. The vias are sized and aligned such that the composite structure extends beyond the fixed end of the cantilevers to ensure that the point of highest tensile stress is not at the boundary between the composite and monolithic silicon. The vias are then etched from the backside by DRIE to release the cantilevers from the wafer. The cantilevers are finally freed from the thin oxide film that covers the via floor by dipping them in hydrofluoric acid, which quickly dissolves the membrane-like film.

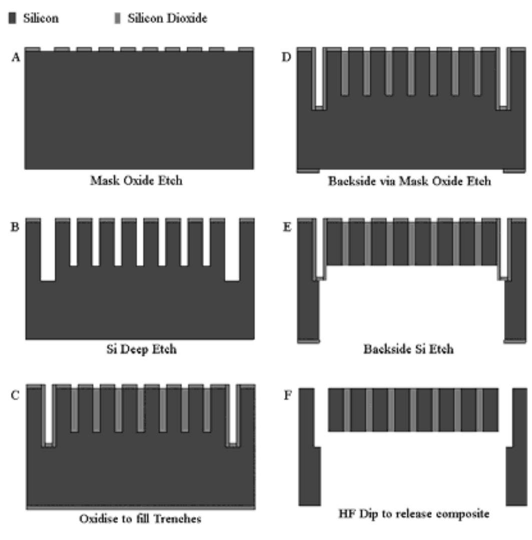

Figure 2: Schematic of fabrication process for composite

3.2 Fracture Testing

Fracture testing on the cantilevers is performed on a modified Tukon microhardness tester, which is well suited for performing fracture testing on these cantilevered samples because testing can be done under load control while keeping the displacement rate as low as desired to avoid any shock loading. The modified indenter consists of a 2mm wide tungsten carbide wedge that allows a uniform load to be applied across the width of the cantilevers. A laser extensometer attached to the instrument enables displacement measurement with up to 1μm accuracy. Loading is done under gravity and varying loads are applied simply by placing different small masses (1-100gm) on top of the indenter. Precise positioning of the samples under the indenter is done with the help of a stereoscopic microscope.

4 RESULTS

The first phase of testing involves verifying the accuracy of the experimental setup and the model to be used to transform the load-to-fracture data into fracture strength data. For this purpose, various loads are applied to the end of the cantilever beams, and the displacement at the point of load application measured to give a load-displacement curve for each sample. A simply supported cantilever beam model, assuming geometric and material linearity is used to obtain the Young's modulus for each sample. The cross section of the cantilevers is assumed to remain uniform over the length, and their height is assumed to correspond to the height as measured from scanning electron micrographs after fracturing one of the samples and imaging the cross section.

The measured values of Young's moduli are shown in Figure 3. The best fit to this data assuming a constant strain model as shown in (2) gives a Young's modulus of 132.8 GPa and 58 GPa for silicon and silicon oxide, respectively.

$$E_{composite} = V_{Si}E_{Si} + V_{Oxide}E_{Oxide} \quad (2)$$

This matches well with the know values for silicon and silicon oxide, and validates our testing procedure.

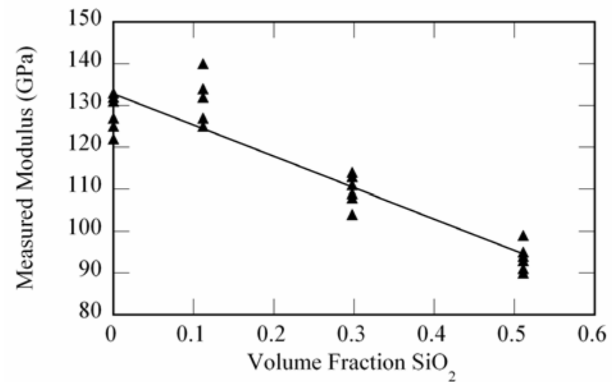

Figure 3: Young's Modulus results for composites with different layer width ratios

Load to fracture measurements are performed on a number of silicon and composite cantilevers to measure fracture strengths. The load is incrementally applied by increasing the mass on the load stage until the sample fractures. The deflection rate is kept at a relatively low value (approximately 7.5μm/sec) to ensure that no fracture occurs due to shock loading.

Initial indications of the efficacy of the laminate geometry with residual compressive stress layers for improved damage tolerance is seen in scanning electron micrographs of the crack path and crack surface on fractured samples as shown in Figure 4. The micrograph shows the crack deflecting each time it crosses the interface between a tensile and compressive layer. Crack deflection is an energy absorbing mechanism, because it creates more

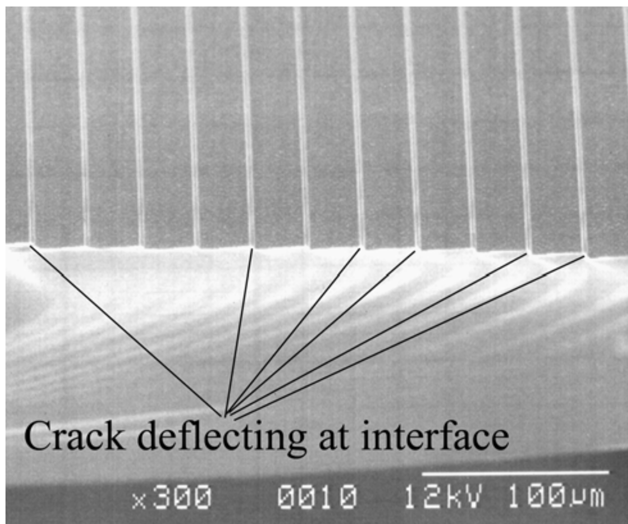

Figure 4: SEM image of fractured composite

surface area in the crack plane than would be formed for a crack growing in a straight line, perpendicular to the laminar structure. Cracks in single crystal silicon grow by cleaving apart adjacent atomic planes, leaving very smooth crack faces. From an energy viewpoint, this represents a higher toughness value G_c for the composite material in comparison to single crystal silicon.

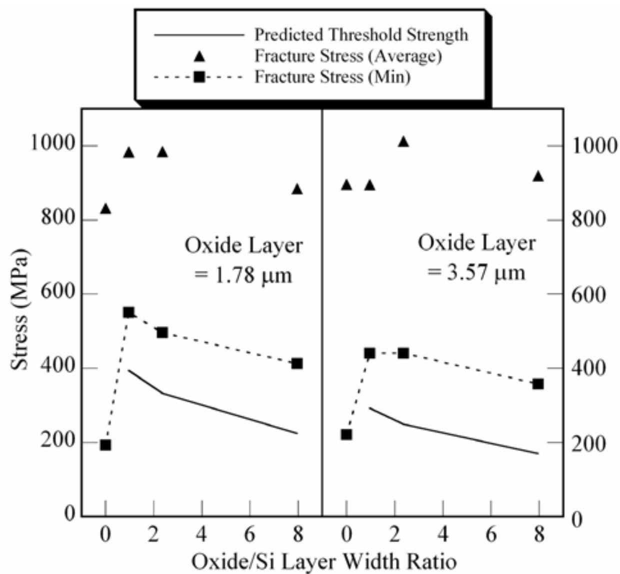

Figure 5: Fracture test data for composites

The data shown in Figure 5 indicates the active presence of a crack arrest phenomenon in the microscale composite structures. SCS cantilevers are shown as composites with the oxide/Si layer width ratio equal to zero. The solid line indicates the threshold stress predicted from the model for composites of different layer width ratios, and the average fracture stress indicated the mean of measured strength for a number of samples of identical composition. It is notable that while the *average* fracture strengths for all the samples lie in a small range, the *minimum* strength has more variance. The minimum measured strength for the composite samples clearly lies above the predicted threshold strength, while the lowest failure stress in SCS is much lower.

A calculation of the flaw size distribution in the SCS samples from the fracture data gives a conservative estimate of 0.1-5 μm. These are reasonable values for flaw sizes in a millimeter scale structure. Two possible sources of these flaws are damage during various processing steps and surface damage due to handling. The measured values for monolithic silicon are also consistent with observations by Johansson [5,6] on the fracture strengths of monolithic silicon cantilevers.

5 CONCLUSIONS

The results obtained from fracture testing of the composite and single crystal silicon cantilevers clearly indicate the presence of a damage tolerance mechanism in the composite material that prevents it from failing below a certain threshold stress. As shown earlier in Figure 1, the threshold stress achievable varies inversely with the size scale of the layer widths. The capability exists for fabricating composites with layer widths between 50-100 nanometers which, according to the model, would only fail under stress levels of 1.8-2 GPa. Preventing failure to such a high level of stress would be invaluable to MEMS designers, since these devices or structures would not require extensive packaging. Another example of application is MEMS devices with comparatively short flexures, since the flexure material would be able to withstand a higher lever of stress. Shorter flexures would reduce the footprint of the device, allowing more devices per chip area. We are currently working on fabricating composites with sub-100 nm layer widths.

REFERENCES

[1] M. P. Rao, A. J. Sanchez-Herencia, G. E. Beltz, R. M. McMeeking, and F. F. Lange, Science **286,** 102-105 (1999).

[2] K. Yasutake, M. Iwata, K. Yoshii, M. Umeno, and H. Kawabe, Journal of Materials Science **21,** 2185-2192 (1986).

[3] T. N. Pornsin-sirirak, Y. C. Tai, H. Nassef, and C. M. Ho, Sensors and Actuators a-Physical **89,** 95-103 (2001).

[4] R. M. McMeeking and K. Hbaieb, Zeitschrift Fur Metallkunde **90,** 1031-1036 (1999).

[5] S. Johansson, F. Ericson, and J. A. Schweitz, Journal of Applied Physics **65,** 122-128 (1989).

[6] S. Johansson, J. A. Schweitz, L. Tenerz, and J. Tiren, Journal of Applied Physics **63,** 4799-4803 (1988).